arXiv:2206.15125v1 [physics.chem-ph] 30 Jun 2022

Core-excited states of SF_6 probed with soft X-ray femtosecond transient absorption of vibrational wavepackets

Lou Barreau,[1,2,*] Andrew D. Ross,[1,2] Victor Kimberg,[3,†] Pavel Krasnov,[4] Svyatoslav Blinov,[4] Daniel M. Neumark,[1,2,‡] and Stephen R. Leone[1,2,5,§]

[1] *Department of Chemistry, University of California, Berkeley, CA, 94720, USA*
[2] *Chemical Sciences Division, Lawrence Berkeley National Laboratory, Berkeley, CA, 94720, USA*
[3] *Department of Theoretical Chemistry and Biology, KTH Royal Institute of Technology, 10691 Stockholm, Sweden*
[4] *International Research Center of Spectroscopy and Quantum Chemistry – IRC SQC, Siberian Federal University, Krasnoyarsk, Russia 660041*
[5] *Department of Physics, University of California, Berkeley, CA, 94720, USA*

(Dated: July 1, 2022)

A vibrational wavepacket in SF_6, created by impulsive stimulated Raman scattering with a few-cycle infrared pulse, is mapped onto five sulfur core-excited states using table-top soft X-ray transient absorption spectroscopy between 170-200 eV. The amplitudes of the X-ray energy shifts of the femtosecond oscillations depend strongly on the nature of the state. The prepared wavepacket is controlled with the pump laser intensity to probe the core-excited levels for various extensions of the S-F stretching motion. This allows the determination of the relative core-level potential energy gradients, in good agreement with TDDFT calculations. This experiment demonstrates a new means of characterizing core-excited potential energy surfaces.

Molecular potential energy surfaces (PESs) dictate the coupled electron-nuclear dynamics following electronic excitation. In particular, PESs of core-excited states are of considerable interest because core-level excitation can induce ultrafast nuclear motion on a timescale shorter than the few-femtosecond core-hole lifetime [1–3]. The X-ray absorption spectrum of a molecule in its vibrational ground state probes only a small region of the PES, at the equilibrium geometry of the ground electronic state. In order to access a larger range of the core-excited PES, multiple infrared (IR) pump - X-ray probe schemes have been theoretically proposed [4–9]; the IR pulse excites the molecule to higher vibrational states where the nuclear wavepacket has a larger spatial extension, so that subsequent absorption of the X-ray pulse can probe regions of the PES that are otherwise inaccessible. The experimental implementation of these proposals requires few-femtosecond to attosecond X-ray pulses, now available at X-ray Free Electron Laser facilities and from table-top sources based on high-order harmonic generation (HHG) [10]. Indeed, X-ray transient absorption spectroscopy is a sensitive probe of structural dynamics [11]; as the geometry changes, the energy of the electronic transition in the X-ray region is modified. This technique has been successfully used to observe vibrational wavepackets in neutral or cationic molecules, often accompanying strong-field ionization in e.g. Br_2 [12, 13], DBr [14], NO [15], CH_3I [16], CH_3Br [17] and C_2H_4 [18], or single-photon and Raman excitation in I_2 [19] and alkyl iodides [20]. In these cases, the vibrational coherence is typically mapped onto a dissociative core-excited state of predominantly $nd^{-1}\sigma^*$ (for halogen-containing species) or $1s^{-1}\pi^*$ character, which corresponds in the single-particle picture to the excitation of a non-bonding core electron to an anti-bonding molecular orbital.

In this letter, we use a combination of IR and soft X-ray (SXR) few-femtosecond pulses to experimentally map a vibrational wavepacket onto five sulfur L-core-excited states of SF_6 in the 170-200 eV energy range (Fig. 1). The IR pump pulse produces a coherent superposition of vibrational states in the ground electronic state by Impulsive Stimulated Raman Scattering (ISRS) [21, 22] and the X-ray absorption energy is probed as a function of the time-delay between the two pulses. The amplitude of the oscillations in energy observed in the transient absorption depends strongly on the core-excited state, in agreement with the nature of the populated molecular orbitals and with Time-Dependent Density Functional Theory (TDDFT) calculations of the core-excited PESs. The intensity of the short IR pulse is used to control the number of vibrational states in the superposition to extract one-dimensional potential energy gradients along a normal mode selected by detection at its vibrational frequency [23].

The SF_6 molecule is chosen for its numerous S 2p core-excited states accessible in the SXR, due to the presence of a shape resonance: $2p_{3/2}^{-1}\ a_{1g}$ and $2p_{1/2}^{-1}\ a_{1g}$ which lie below the respective 2p ionization potentials at 172.27 and 173.44 eV respectively, and $2p_{3/2}^{-1}\ t_{2g}$, $2p_{1/2}^{-1}\ t_{2g}$ and $2p^{-1}\ e_g$ located in the shape resonance at 183.40, 184.57 and 196.2 eV respectively [24, 25]. This polyatomic molecule possesses fifteen vibrational modes but due to its high symmetry many of them are degenerate.

* Present address: Institut des Sciences Moléculaires d'Orsay, UMR 8214, CNRS, Université Paris-Saclay, Bâtiment 520, 91405 Orsay Cedex, France.; lou.barreau@universite-paris-saclay.fr
† kimberg@kth.se
‡ dneumark@berkeley.edu
§ srl@berkeley.edu

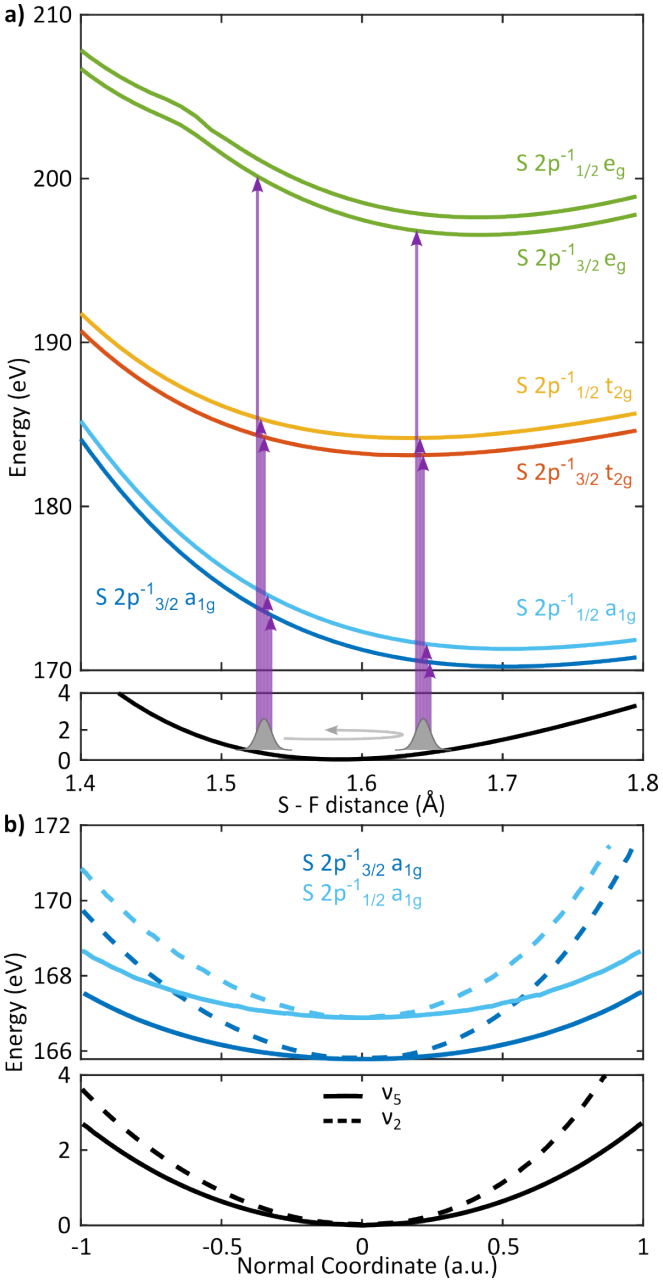


FIG. 1. **a)** Illustrative schematic of the experiment principle overlaid on the calculated ground (bottom, black) and core-excited (top) states potential energy curves along the ν_1 mode. **b)** Same as a) along the ν_2 (dashed line) and ν_5 (full line) modes. Only the $2p^{-1}$ a_{1g} states are shown because these vibrational modes lift the degeneracy of the $2p^{-1}$ t_{2g} and $2p^{-1}$ e_g states outside the equilibrium geometry.

Among those, three are Raman-active [26]: the symmetric stretch ν_1 ($\nu_1 = 775$ cm^{-1}, $T_1 = 43$ fs), antisymmetric stretch ν_2 ($\nu_2 = 643$ cm^{-1}, $T_2 = 52$ fs), and bend ν_5 ($\nu_5 = 525$ cm^{-1}, $T_5 = 63$ fs). They can be excited by ISRS with IR pulses shorter than their vibrational period, and the corresponding multimode wavepacket dynamics have been characterized with high-harmonic spectroscopy [27–30]. Figure 1 shows the relevant ground and core-excited potential energy curves calculated by, respectively, DFT [31] and TDDFT [32] methods using the ORCA software [33] with B3LYP functional [34–36], ano-pVTZ basis set [37], RI approximation [38] and quasi-degenerated perturbation theory [39] for spin-orbit coupling inclusion. Preliminarily, the geometry and vibrational modes of SF_6 were calculated by DFT under O_h symmetry constrained with the help of the GAMESS software [40] using the B3LYP functional and def2-TZVP basis set [41].

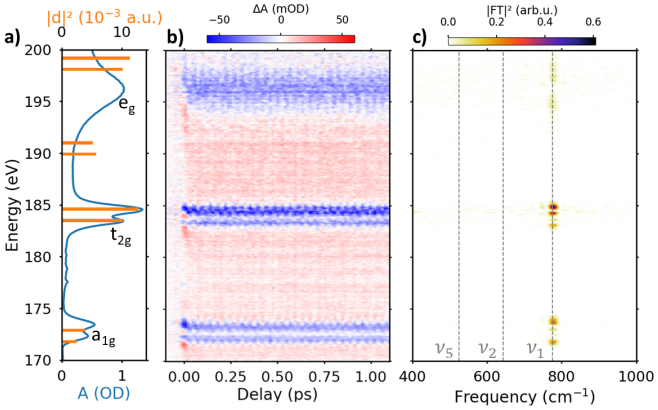


FIG. 2. **a)** Measured (blue) and calculated (orange) SF_6 absorption spectrum at the S $L_{2,3}$ edge. The pre-edge background absorption has been subtracted in the measurement. The calculated energies are shifted by +6.0 eV. The additional doublet of e_g symmetry calculated around 190 eV is not observed in the experiment. **b)** Transient absorption spectrogram. Positive delays correspond to the SXR pulse following the vis-NIR pulse. **c)** Squared Fourier transform of **b**. Frequencies of the ν_1, ν_2 and ν_5 modes are indicated as vertical dashed lines.

The experimental setup has been described elsewhere [42]. Briefly, 85% of the energy of a commercial Ti:sapphire laser delivering 13 mJ, 30 fs, 800 nm pulses is used to pump a multistage optical parametric amplifier that converts the wavelength to 1300 nm. The resulting short-wave infrared (SWIR) pulses are compressed to 12.8 fs full-width at half-maximum (fwhm) with a hollow-core fiber (HCF) compressor, and focused into a semi-infinite gas cell filled with 2 bar of flowing helium for HHG. This yields SXR pulses with a continuous spectrum extending up to 370 eV. The remaining SWIR light is filtered out with a Sn film, and the SXR pulses are focused by a toroidal mirror into a gas cell filled with 25 mbar of SF_6. The SXR spectrum I is measured after dispersion on a grating and imaging on an X-ray CCD camera. The absorbance A is defined as $A = -\log_{10}(I/I_0)$, where I_0 is the spectrum measured without sample.

In the time-resolved experiments, the remaining 2 mJ, 800 nm pulses are simultaneously compressed in a second HCF compressor to produce 0.75 mJ, 6 fs pulses in the visible-near IR (vis-NIR). After propagation in a piezo-controlled delay line, the vis-NIR pulses are focused with a $f = 37.5$ cm mirror into the gas cell to excite the

molecules. The change in absorbance at a delay τ after the pump vis-NIR pulse is $\Delta A(\tau) = -\log_{10}(I_{\rm on}(\tau)/I_{\rm off})$, where $I_{\rm on}$ and $I_{\rm off}$ are the spectra measured with and without the pump pulse at each delay, respectively. The ensemble of pump-off spectra is used for the edge-pixel referencing technique applied to reduce the SXR fluctuations noise in the transient absorption data [43]. In this all-optical experiment, the time and energy resolutions are not interdependent through the uncertainty principle (as opposed to core-level photoelectron spectroscopy that was proposed in [44] to probe SF_6 vibrations) so that they can be both optimally short and narrow, respectively.

Figure 2a shows the absorption spectrum of SF_6 in the vicinity of the S L-edge measured in the absence of the vis-NIR pulse (blue curve). Five peaks are observed, corresponding to the excitation to the spin-orbit split S $2p^{-1}$ a_{1g} and S $2p^{-1}$ t_{2g} states as well as a broad band attributed to the S $2p^{-1}$ e_g doublet, in agreement with reported synchrotron data [24] and our B3LYP TDDFT calculations (orange sticks). Our discussion focuses now on the dynamics outside of the temporal overlap of the pulses, as opposed to the recent work of Rupprecht *et al.* [45]. The transient absorption of SF_6 after excitation by the $\approx 6\times10^{14}$ W/cm^2 vis-NIR pulse is shown in Fig. 2b. Clear oscillations of the absorbance are observed at positive delays for the five peaks with a period of ≈ 43 fs. The oscillations are long-lived, and the Fourier transform in Fig. 2c reveals a single feature at 775 cm^{-1} corresponding to the ν_1 vibrational mode, visible at the energies of all the core-excited levels. With short pump pulses in this intensity range, previous work showed that the three Raman-active modes can be simultaneously excited [27–30], but only one is observed here. The positive features appearing at positive delays in-between the assigned peaks in Fig. 2b may be attributed to strong-field dissociation of SF_6, although they differ in shape from what was observed in [46]. Bands attributed to the formation of SF_5^+ in Ref. [46] were not observed under our experimental conditions, despite our higher spectral resolution.

Mapping the same vibrational coherence onto five different core-excited states allows us to compare them. To quantitatively characterize the PES gradients of the five states for the ν_1 normal mode, we use the vis-NIR pump intensity to control the number of vibrational states included in the superposition and therefore the nuclear wavepacket. For ISRS excitation with an electric field $\mathcal{E}$, the nuclear wavefunction $\chi(q,t)$ satisfies the time-dependent Schrödinger equation (in atomic units):

$$i\frac{\partial\chi(q,t)}{\partial t} = \left(-\frac{1}{2\mu}\frac{\partial^2}{\partial q^2} + V(q) - \frac{1}{2}\sum_{i,j}\alpha_{ij}(q)\mathcal{E}_i(t)\mathcal{E}_j(t)\right)\chi(q,t) \qquad (1)$$

where μ is the reduced mass of the normal mode, V the ground state PES, α the polarizability tensor and $\mathcal{E}_i$ the amplitude of the electric field of the laser pulse along the i axis. For the symmetric stretch mode ν_1 the normal coordinate q identifies with the S-F distance. Figure 3a displays the squared nuclear wavepacket $|\chi(q,t)|^2$ in the ground state found from the numerical solution of Eq.(1) with a 6×10^{14} W/cm^2, 6 fs fwhm Gaussian pump

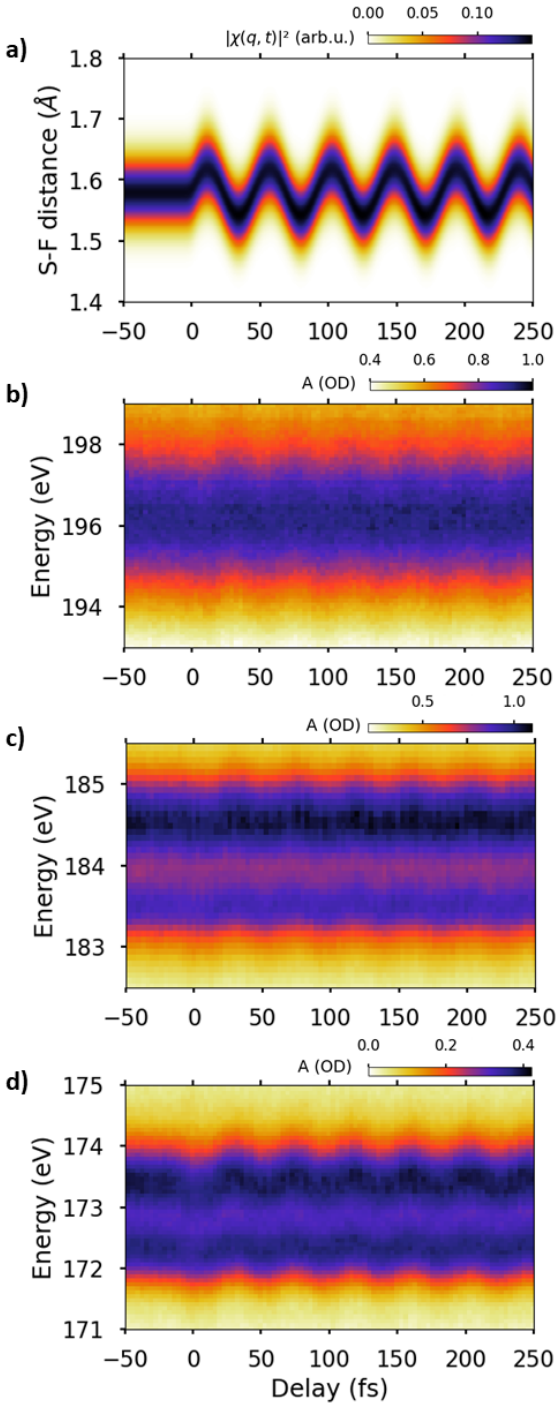


FIG. 3. **a)** Simulated nuclear wavepacket after ISRS excitation of the ν_1 mode by a 6 fs, 800 nm pulse of intensity 6×10^{14} W/cm^2. **b-d)** Measured absorbance $A(\tau)$ for the five core-excited states at the same pump intensity.

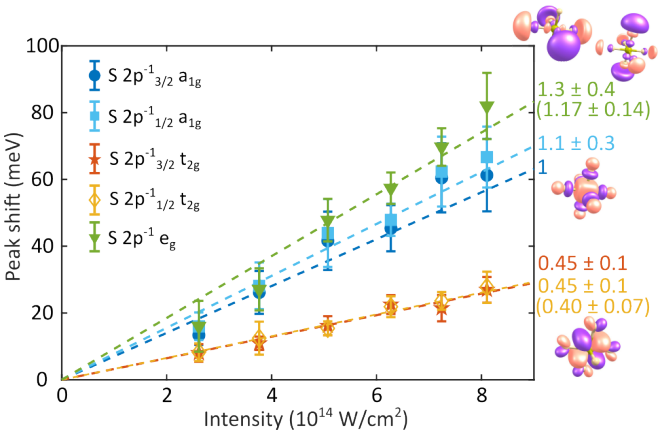


FIG. 4. Amplitude of the absorption peak shift as a function of the pump intensity for the five S core-excited states and their linear fit (dashed line). The error bars represent the 95 % confidence bounds. The relative slopes are indicated on the right, with numbers in parenthesis obtained from a fitting procedure including other data sets described in [47, 48]. Illustrations of the e_g, a_{1g} and t_{2g} molecular orbitals are shown next to the corresponding state.

pulse and α and $V(q)$ extracted from DFT B3LYP/def2-TZVP quantum-chemical simulations under constrained O_h symmetry with the GAMESS software. The theoretical PES results in a smaller vibrational frequency than the tabulated value (728 cm^{-1}), giving a slightly longer period of the wavepacket oscillations in Fig. 3a compared to the experiment. At this pump intensity, vibrational levels up to $\nu_1 = 3$ are populated by ISRS [48], and the S-F distance changes by ±2.4 %. As the center of the wavepacket oscillates, it is mapped onto the five core-excited PESs. The absorbance measured after excitation with the 6×10^{14} W/cm^2 vis-NIR pulse with 3 fs delay steps is shown in Fig. 3b-d. Apart from a slight difference in frequency originating from the calculated ground state potential, the absorbance oscillations nicely follow the nuclear wavepacket. At each delay, the absorption features are fitted by a Gaussian or Lorentzian function depending on the core-excited state [24]. Their central energy oscillates as a function of the vis-NIR - SXR delay with a period of $T_1 = 43$ fs. The oscillations of the central energy are then fitted to a cosine function. Their amplitudes are different for the five core-excited states and inform on their relative PES gradients. The vis-NIR pump intensity is varied with a broadband combination of half-waveplate and polarizer between 2.6×10^{14} and 8×10^{14} W/cm^2. This allows us to incorporate greater or fewer vibrational states in the coherent superposition. Calculations show that the nuclear wavepacket spatial excursion is linear with the laser intensity in this range[48]. A SXR transient absorption spectrogram is measured for six different intensities, all other parameters remaining identical. The amplitude of the central energy oscillation for the five core-excited states at each pump intensity is reported in Fig. 4. For the same nuclear geometry change in the ground state (i.e. at a given pump intensity), the SXR transition energies to the S 2p^{-1} a_{1g} and S 2p^{-1} e_g states have wider excursions from the equilibrium geometry transition compared to the S 2p^{-1} t_{2g} state. This result reveals the larger displacement of the PES along the S-F bond upon excitation to the S 2p^{-1} a_{1g} and S 2p^{-1} e_g states compared to S 2p^{-1} t_{2g}. This different behavior reflects the non-bonding character of the t_{2g} molecular orbital, whereas both the a_{1g} and e_g orbitals are anti-bonding along the S-F bonds (Fig. 4) therefore the electronic energy is more dependent on the internuclear distance.

More quantitatively, the linear increases of the energy shifts with the pump intensity - which is the spatial extension of the nuclear wavefunction - can be extracted from a fit of Fig. 4. These shifts are directly related to the gradients of the PESs along the S-F distance. With the lowest core-excited state S 2p$^{-1}_{3/2}$ a_{1g} taken as a reference, the relative PESs gradients are 1.1 ± 0.3 (S 2p$^{-1}_{1/2}$ a_{1g}), 0.45 ± 0.1 (S 2p$^{-1}_{3/2}$ t_{2g}), 0.45 ± 0.1 (S 2p$^{-1}_{1/2}$ t_{2g}), and 1.3 ± 0.4 (S 2p^{-1} e_g) (Fig. 4). The results are consistent with the calculated PESs presented in Fig. 1. As typically observed for core-excited states [3], these PESs have steep gradients along the symmetric stretch mode ν_1, of the order of 10 to 30 eV/Å. At the equilibrium geometry, the gradients of the calculated PESs relative to S 2p$^{-1}_{3/2}$ a_{1g} are 1.01 (S 2p$^{-1}_{1/2}$ a_{1g}), 0.38 (S 2p$^{-1}_{3/2}$ t_{2g}), 0.38 (S 2p$^{-1}_{1/2}$ t_{2g}), 1.05 (S 2p$^{-1}_{3/2}$ $2e_g$), and 1.05 (S 2p$^{-1}_{1/2}$ $2e_g$), in good agreement with the experimental values. The spectral broadening caused by the large gradient and additional spectral background of multielectron character [49] does not allow the resolution of the e_g doublet in practice. The calculated PESs for the ground state and the two lowest core-excited states of a_{1g} symmetry along the normal coordinates of the two other Raman-active modes (ν_2 and ν_5) are shown in Fig. 1b. The core-excited and ground states are relatively parallel, confirming the lack of observed oscillations in the experiment. A similar behaviour is expected for the higher e_g and t_{2g} core-excited states, but vibrations along the non-totally symmetric ν_2 and ν_5 modes lift the degeneracy of these states, making the calculations of the PESs more complex and beyond the scope of this work.

Vibrational dynamics resulting from strong-field ionization have previously been observed with X-ray transient absorption spectroscopy [12–18]. Here, the use of ISRS excitation provides a controlled vibrational wavepacket in the ground electronic state of the molecule. This in turn enables the characterization of multiple core-excited PESs. These results are an experimental demonstration of how to probe different regions of the core-excited PESs with the IR pump/X-ray probe scheme theoretically proposed over fifteen years ago [4–6]. Taking advantage of the element specificity of X-ray spectroscopy, multidimensional unexplored regions of core-excited PESs in many systems are accessible with this scheme, implemented either on table-top sources

of femtosecond X-ray pulses or Free Electron Lasers. These unexplored regions are expected to drive nuclear dynamics, such as proton transfer in oxygen-core-excited water dimers [6], and could therefore be used to control chemical reactions in short-lived core-excited states.

The authors acknowledge fruitful discussions with Yann Mairesse and Marc Simon. This work is supported by the Gas Phase Chemical Physics program of the U.S. Department of Energy, Office of Science, Office of Basic Energy Sciences, Chemical Sciences, Geosciences and Biosciences Division (DE-AC02-05CH11231, FWP no. CHPHYS01 (D.M.N., S.R.L.)), the National Science Foundation (Grant No. CHE-1951317 and No. CHE-1660417 (S.R.L.), NSF MRI 1624322 for equipment and A.D.R.), the U.S. Army Research Office under Grant No. W911NF-14-1-0383 (D.M.N., S.R.L.). A.D.R. is also supported by the U.S. Army Research Office Grant No. W011NF-20-1-0127 (D.M.N.) and the W.M. Keck Foundation Grant No. 042982 (S.R.L.). V.K. acknowledges support from the Swedish Research Council (VR) project No. 2019-03470. P.K. and S.B. acknowledge Russian Foundation for Basic Research (RFBR), Project No. 19-29-12015. L.B. acknowledges support from the Miller Institute for Basic Research in Science at UC Berkeley.

[1] F. Gelmukhanov and H. Ågren, X-ray resonant scattering involving dissociative states, Phys. Rev. A **54**, 379 (1996).

[2] M. Simon, C. Miron, N. Leclercq, P. Morin, K. Ueda, Y. Sato, S. Tanaka, and Y. Kayanuma, Nuclear motion of core excited BF_3 probed by high resolution resonant auger spectroscopy, Phys. Rev. Lett. **79**, 3857 (1997).

[3] T. Marchenko, G. Goldsztejn, K. Jänkälä, O. Travnikova, L. Journel, R. Guillemin, N. Sisourat, D. Céolin, M. Žitnik, M. Kavčič, K. Bučar, A. Mihelič, B. C. de Miranda, I. Ismail, A. F. Lago, F. Gel'mukhanov, R. Püttner, M. N. Piancastelli, and M. Simon, Potential energy surface reconstruction and lifetime determination of molecular double-core-hole states in the hard x-ray regime, Phys. Rev. Lett. **119**, 133001 (2017).

[4] V. C. Felicíssimo, F. F. Guimarães, and F. Gel'mukhanov, Enhancement of the recoil effect in X-ray photoelectron spectra of molecules driven by a strong IR field, Phys. Rev. A **72**, 023414 (2005).

[5] F. F. Guimarães, V. Kimberg, V. C. Felicíssimo, F. Gel'mukhanov, A. Cesar, and H. Ågren, Infrared–x-ray pump-probe spectroscopy of the NO molecule, Phys. Rev. A **72**, 012714 (2005).

[6] V. C. Felicissimo, F. F. Guimaraes, F. Gel'mukhanov, A. Cesar, and H. Ågren, The principles of infrared-X-ray pump-probe spectroscopy. applications on proton transfer in core-ionized water dimers, The Journal of chemical physics **122**, 094319 (2005).

[7] S. Carniato, R. Taïeb, R. Guillemin, L. Journel, M. Simon, and F. Gel'mukhanov, K-L resonant X-ray Raman scattering as a tool for potential energy surface mapping, Chemical physics letters **439**, 402 (2007).

[8] S. Engin, N. Sisourat, P. Selles, R. Taïeb, and S. Carniato, Probing IR-Raman vibrationally excited molecules with X-ray spectroscopy, Chemical Physics Letters **535**, 192 (2012).

[9] N. Ignatova, V. V. da Cruz, R. C. Couto, E. Ertan, M. Odelius, H. Ågren, F. F. Guimarães, A. Zimin, S. P. Polyutov, F. Gel'mukhanov, and V. Kimberg, Infrared-pump–x-ray-probe spectroscopy of vibrationally excited molecules, Phys. Rev. A **95**, 042502 (2017).

[10] L. Young, K. Ueda, M. Gühr, P. H. Bucksbaum, M. Simon, S. Mukamel, N. Rohringer, K. C. Prince, C. Masciovecchio, M. Meyer, *et al.*, Roadmap of ultrafast X-ray atomic and molecular physics, Journal of Physics B: Atomic, Molecular and Optical Physics **51**, 032003 (2018).

[11] R. Geneaux, H. J. Marroux, A. Guggenmos, D. M. Neumark, and S. R. Leone, Transient absorption spectroscopy using high harmonic generation: a review of ultrafast X-ray dynamics in molecules and solids, Philosophical Transactions of the Royal Society A **377**, 20170463 (2019).

[12] E. R. Hosler and S. R. Leone, Characterization of vibrational wave packets by core-level high-harmonic transient absorption spectroscopy, Phys. Rev. A **88**, 023420 (2013).

[13] Y. Kobayashi, K. F. Chang, S. M. Poullain, V. Scutelnic, T. Zeng, D. M. Neumark, and S. R. Leone, Coherent electronic-vibrational dynamics in deuterium bromide probed via attosecond transient-absorption spectroscopy, Phys. Rev. A **101**, 063414 (2020).

[14] Y. Kobayashi, D. M. Neumark, and S. R. Leone, Attosecond XUV probing of vibronic quantum superpositions in Br_2^+, Phys. Rev. A **102**, 051102 (2020).

[15] N. Saito, H. Sannohe, N. Ishii, T. Kanai, N. Kosugi, Y. Wu, A. Chew, S. Han, Z. Chang, and J. Itatani, Real-time observation of electronic, vibrational, and rotational dynamics in nitric oxide with attosecond soft X-ray pulses at 400 eV, Optica **6**, 1542 (2019).

[16] Z. Wei, J. Li, L. Wang, S. T. See, M. H. Jhon, Y. Zhang, F. Shi, M. Yang, and Z.-H. Loh, Elucidating the origins of multimode vibrational coherences of polyatomic molecules induced by intense laser fields, Nature communications **8**, 1 (2017).

[17] H. Timmers, X. Zhu, Z. Li, Y. Kobayashi, M. Sabbar, M. Hollstein, M. Reduzzi, T. J. Martínez, D. M. Neumark, and S. R. Leone, Disentangling conical intersection and coherent molecular dynamics in methyl bromide with attosecond transient absorption spectroscopy, Nature communications **10**, 1 (2019).

[18] K. S. Zinchenko, F. Ardana-Lamas, I. Seidu, S. P. Neville, J. van der Veen, V. U. Lanfaloni, M. S. Schuurman, and H. J. Wörner, Sub-7-femtosecond conical-intersection dynamics probed at the carbon k-edge, Science **371**, 489 (2021).

[19] S. M. Poullain, Y. Kobayashi, K. F. Chang, and S. R. Leone, Visualizing coherent vibrational motion in the molecular iodine $b\,^3\Pi_{0^+_u}$ state using ultrafast xuv transient-absorption spectroscopy, Phys. Rev. A **104**, 022817 (2021).

[20] K. F. Chang, H. Wang, S. M. Poullain, J. González-Vázquez, L. Bañares, D. Prendergast, D. M. Neumark, and S. R. Leone, Conical intersection and coherent vibrational dynamics in alkyl iodides captured by attosecond transient absorption spectroscopy, The Journal of Chemical Physics **156**, 114304 (2022).

[21] Y.-X. Yan, E. B. Gamble Jr, and K. A. Nelson, Impulsive stimulated scattering: General importance in femtosecond laser pulse interactions with matter, and spectroscopic applications, The Journal of chemical physics **83**, 5391 (1985).

[22] Y.-X. Yan and K. A. Nelson, Impulsive stimulated light scattering. i. general theory, The Journal of chemical physics **87**, 6240 (1987).

[23] S. Gerber, S.-L. Yang, D. Zhu, H. Soifer, J. Sobota, S. Rebec, J. Lee, T. Jia, B. Moritz, C. Jia, *et al.*, Femtosecond electron-phonon lock-in by photoemission and X-ray free-electron laser, Science **357**, 71 (2017).

[24] E. Hudson, D. A. Shirley, M. Domke, G. Remmers, A. Puschmann, T. Mandel, C. Xue, and G. Kaindl, High-resolution measurements of near-edge resonances in the core-level photoionization spectra of SF_6, Phys. Rev. A **47**, 361 (1993).

[25] M. Stener, P. Bolognesi, M. Coreno, P. O'Keeffe, V. Feyer, G. Fronzoni, P. Decleva, L. Avaldi, and A. Kivimäki, Photoabsorption and S 2p photoionization of the SF_6 molecule: Resonances in the excitation energy range of 200–280 ev, The Journal of chemical physics **134**, 174311 (2011).

[26] H. H. Claassen, G. L. Goodman, J. H. Holloway, and H. Selig, Raman spectra of MoF_6, TcF_6, ReF_6, UF_6, SF_6, SeF_6, and TeF_6 in the vapor state, The Journal of Chemical Physics **53**, 341 (1970).

[27] N. L. Wagner, A. Wüest, I. P. Christov, T. Popmintchev, X. Zhou, M. M. Murnane, and H. C. Kapteyn, Monitoring molecular dynamics using coherent electrons from high harmonic generation, Proceedings of the National Academy of Sciences **103**, 13279 (2006).

[28] A. Ferré, D. Staedter, F. Burgy, M. Dagan, D. Descamps, N. Dudovich, S. Petit, H. Soifer, V. Blanchet, and Y. Mairesse, High-order harmonic transient grating spectroscopy of SF_6 molecular vibrations, Journal of Physics B: Atomic, Molecular and Optical Physics **47**, 124023 (2014).

[29] A. Ferré, A. Boguslavskiy, M. Dagan, V. Blanchet, B. Bruner, F. Burgy, A. Camper, D. Descamps, B. Fabre, N. Fedorov, *et al.*, Multi-channel electronic and vibrational dynamics in polyatomic resonant high-order harmonic generation, Nature communications **6**, 1 (2015).

[30] D. Baykusheva, M. S. Ahsan, N. Lin, and H. J. Wörner, Bicircular high-harmonic spectroscopy reveals dynamical symmetries of atoms and molecules, Phys. Rev. Lett. **116**, 123001 (2016).

[31] P. Hohenberg and W. Kohn, Inhomogeneous electron gas, Phys. Rev. **136**, B864 (1964).

[32] E. Runge and E. K. U. Gross, Density-functional theory for time-dependent systems, Phys. Rev. Lett. **52**, 997 (1984).

[33] F. Neese, Software update: the orca program system, version 4.0, WIREs Computational Molecular Science **8**, e1327 (2018).

[34] A. D. Becke, Density-functional thermochemistry. iii. the role of exact exchange, The Journal of Chemical Physics **98**, 5648 (1993).

[35] C. Lee, W. Yang, and R. G. Parr, Development of the colle-salvetti correlation-energy formula into a functional of the electron density, Phys. Rev. B **37**, 785 (1988).

[36] S. H. Vosko, L. Wilk, and M. Nusair, Accurate spin-dependent electron liquid correlation energies for local spin density calculations: a critical analysis, Canadian Journal of physics **58**, 1200 (1980).

[37] F. Neese and E. F. Valeev, Revisiting the atomic natural orbital approach for basis sets: Robust systematic basis sets for explicitly correlated and conventional correlated ab initio methods?, Journal of Chemical Theory and Computation **7**, 33 (2011), pMID: 26606216.

[38] R. Kendall and H. Früchtl, The impact of the resolution of the identity approximate integral method on modern ab initio algorithm development, Theor Chem Acta **97**, 158–163 (1997).

[39] B. de Souza, G. Farias, F. Neese, and R. Izsák, Predicting phosphorescence rates of light organic molecules using time-dependent density functional theory and the path integral approach to dynamics, Journal of Chemical Theory and Computation **15**, 1896 (2019).

[40] M. W. Schmidt, K. K. Baldridge, J. A. Boatz, S. T. Elbert, M. S. Gordon, J. H. Jensen, S. Koseki, N. Matsunaga, K. A. Nguyen, S. Su, T. L. Windus, M. Dupuis, and J. A. Montgomery Jr, General atomic and molecular electronic structure system, Journal of Computational Chemistry **14**, 1347 (1993).

[41] F. Weigend and R. Ahlrichs, Balanced basis sets of split valence, triple zeta valence and quadruple zeta valence quality for h to rn: Design and assessment of accuracy, Phys. Chem. Chem. Phys. **7**, 3297 (2005).

[42] L. Barreau, A. D. Ross, S. Garg, P. M. Kraus, D. M. Neumark, and S. R. Leone, Efficient table-top dual-wavelength beamline for ultrafast transient absorption spectroscopy in the soft X-ray region, Scientific reports **10**, 1 (2020).

[43] R. Géneaux, H.-T. Chang, A. M. Schwartzberg, and H. J. Marroux, Source noise suppression in attosecond transient absorption spectroscopy by edge-pixel referencing, Optics Express **29**, 951 (2021).

[44] N.-T. Nguyen, R. R. Lucchese, C. D. Lin, and A.-T. Le, Probing and extracting the structure of vibrating SF_6 molecules with inner-shell photoelectrons, Phys. Rev. A **93**, 063419 (2016).

[45] P. Rupprecht, L. Aufleger, S. Heinze, A. Magunia, T. Ding, M. Rebholz, S. Amberg, N. Mollov, F. Henrich, M. W. Haverkort, C. Ott, and T. Pfeifer, Laser control of electronic exchange interaction within a molecule, Phys. Rev. Lett. **128**, 153001 (2022).

[46] Y. Pertot, C. Schmidt, M. Matthews, A. Chauvet, M. Huppert, V. Svoboda, A. von Conta, A. Tehlar, D. Baykusheva, J.-P. Wolf, *et al.*, Time-resolved X-ray absorption spectroscopy with a water window high-harmonic source, Science **355**, 264 (2017).

[47] A. D. Ross, D. Hait, V. Scutelnic, E. A. Haugen, E. Ridente, M. B. Balkew, D. M. Neumark, M. Head-Gordon, and S. R. Leone, Jahn-Teller distortion and dissociation of CCl_4^+ by transient X-ray spectroscopy simultaneously at the carbon K- and chlorine L-edge, arXiv 10.48550/ARXIV.2204.13800 (2022).

[48] See Supplemental Material.

[49] A. Kivimäki, M. Coreno, P. Miotti, F. Frassetto, L. Poletto, C. Stråhlman, M. De Simone, and R. Richter, The multielectron character of the S 2p→ 4eg shape resonance

in the sf_6 molecule studied via detection of softX-ray emission and neutral high-rydberg fragments, Journal of Electron Spectroscopy and Related Phenomena **209**, 26 (2016).